Room-Temperature Long-Range Ferromagnetic Order in a Confined Molecular Monolayer

Yuhua Liu
University of Science and Technology of China
Haifeng Lv
University of Science and Technology of China
Bingkai Yuan
University of Science and Technology of China
Yuqiao Guo
University of Science and Technology of China
Yue Lin
University of Science and Technology of China
Xiaolin Tai
University of Science and Technology of China
Yongliang Qin
Anhui Province Key Laboratory of Condensed Matter Physics at Extreme Conditions
Jing Peng
University of Science and Technology of China
Jiyin Zhao
University of Science and Technology of China
Yueqi Su
University of Science and Technology of China
Yang Liu
University of Science and Technology of China
Wangsheng Chu
University of Science and Technology of China
Xiaojun Wu
University of Science and Technology of China https://orcid.org/0000-0003-3606-1211
Changzheng Wu (czwu@ustc.edu.cn)
University of Science and Technology of China https://orcid.org/0000-0002-4416-6358
Yi Xie
University of Science and Technology of China

Article

Keywords:

Posted Date: September 12th, 2022

DOI: https://doi.org/10.21203/rs.3.rs-2031838/v1

Room-Temperature Long-Range Ferromagnetic Order in a Confined Molecular Monolayer

Yuhua Liu[1†], Haifeng Lv[1†], Bingkai Yuan[1†], Yuqiao Guo[1,2 *], Yue Lin[1], Xiaolin Tai[1], Yongliang Qin[3], Jing Peng[1], Jiyin Zhao[1], Yueqi Su[1], Yang Liu[1], Wangsheng Chu[1], Xiaojun Wu[1*], Changzheng Wu[1,2*] and Yi Xie[1,2]

1 School of Chemistry and Materials Science, CAS Center for Excellence in Nanoscience, CAS Key Laboratory of Mechanical Behavior and Design of Materials, and National Synchrotron Radiation Laboratory, University of Science & Technology of China, Hefei 230026, P. R. China.
2 Institute of Energy, Hefei Comprehensive National Science Center. Hefei, Anhui 230031, P. R. China.
3 Anhui Province Key Laboratory of Condensed Matter Physics at Extreme Conditions, High Magnetic Field Laboratory, Chinese Academy of Sciences, Hefei 230031, P. R. China.
† These authors contributed equally: Yuhua Liu, Haifeng Lv, Bingkai Yuan.
* Corresponding Authors. E-mails: czwu@ustc.edu.cn, guoyq@ustc.edu.cn, xjwu@ustc.edu.cn

Abstract: Pursuing new ferromagnetic systems could bring about research breakthroughs for magnetism. Currently, studies of magnetic ordering are expanding from interatomic to intermolecular exchange interactions to produce ferromagnets in inorganic/organic crystals[1-3]. To date, the crystalline framework used for stabilizing parallel spin alignment via an ordered lattice seems to be indispensable to ferromagnetism[4]. In our case, we demonstrated room-temperature long-range ferromagnetic order in two-dimensional confined cobaltocene ($Co(Cp)_2$) molecular monolayers. In a confined van der Waals (vdW) interlayer space, spontaneous uniform spin orientation of $Co(Cp)_2$ can be settled. Ferromagnetic coupling is established by an intermolecular vibronic superexchange interaction[4,5], a new long-distance exchange interaction in a cooperative dynamic Jahn-Teller (J-T)[5,6] $Co(Cp)_2$ monolayer. As expected, the confined $Co(Cp)_2$ monolayers exhibit a high ferromagnetic transition temperature (above room temperature) with a saturation magnetization up to 4 $emu.g^{-1}$.

The origin of ferromagnetism, *i.e.*, spontaneous parallel spin ordering[7,8], has been a long-standing pursuit of scientists. The spin-spin exchange interaction is the essential factor for ferromagnetic ordering[9-12], which determines the ferromagnetic properties of a material, such as the transition temperature (T_c) and saturation magnetization (M_s). As the exchange interaction is extremely sensitive to the distance of adjacent spins[13], ferromagnetism can restrictedly be found in a crystalline framework. Through translational symmetry, a crystalline framework with a uniform distance between adjacent lattice sites provides ideal conditions for spin ordering. Therefore, conventional ferromagnets with high T_c and large M_s are found in highly crystalline inorganic systems with strongly bonded atoms, ranging from transition metals to lanthanide metals[14,15] and their oxides with perovskite and spinel structures[16-18].

Magnetic molecules are a new class of magnetic moment units of great potential interest, and currently, pursuing magnetic order in molecular systems, especially two-dimensional (2D) system beyond room

temperature is a very important research area. Different from conventional ferromagnetic systems relying on the exchange interaction of unpaired electrons of d or f shells, for molecular systems, the cooperative spin-spin exchange interaction to achieve ferromagnetic coupling is usually based on their p shells or π-π stacking[19,20], which enlarges the distance of the exchange interaction between the local magnetic moments. The long-distance exchange interaction in molecular systems brings a new system of ferromagnetic ordering beyond inorganic crystals, such as the Prussian blue framework[21] and metal-organic frameworks (MOFs)[22]. However, for molecular systems, a stable crystalline lattice is still indispensable to achieve ferromagnets with long-range ferromagnetic order. In fact, high-temperature ferromagnetic order is strongly dependent on stable lattice constraints for resistance to thermal agitation, which is more vulnerable in atomic limit[23,24]. Therefore, challenges still remain in robust ferromagnetic ordering of independent molecules and their aggregates in 2D limit, which have no stable crystalline lattice. And a new exchange interaction is required for long-range ferromagnetic order in molecular aggregate systems, which is vital for not only fundamentally understanding the nature of magnetism but also opening new avenues towards a new magnetic material platform.

Herein, we achieved room-temperature long-range ferromagnetic order in a confined molecular monolayer as a new class of ferromagnetic configurations under atomic thickness. A molecular monolayer of $Co(Cp)_2$ can be achieved in a confined van der Waals (vdW) interlayer space. An intermolecular vibronic superexchange interaction, as a new exchange interaction induced by the cooperative vibronic Jahn-Teller (J-T) effect, produces strong ferromagnetic coupling between $Co(Cp)_2$ molecules and realizes high T_c (> 300 K) and large M_s (4 $emu.g^{-1}$). The construction of robust intermolecular ferromagnetic coupling among 2D confined molecular aggregates will promote the understanding of the ferromagnetic mechanism and the search for low-dimensional ferromagnets.

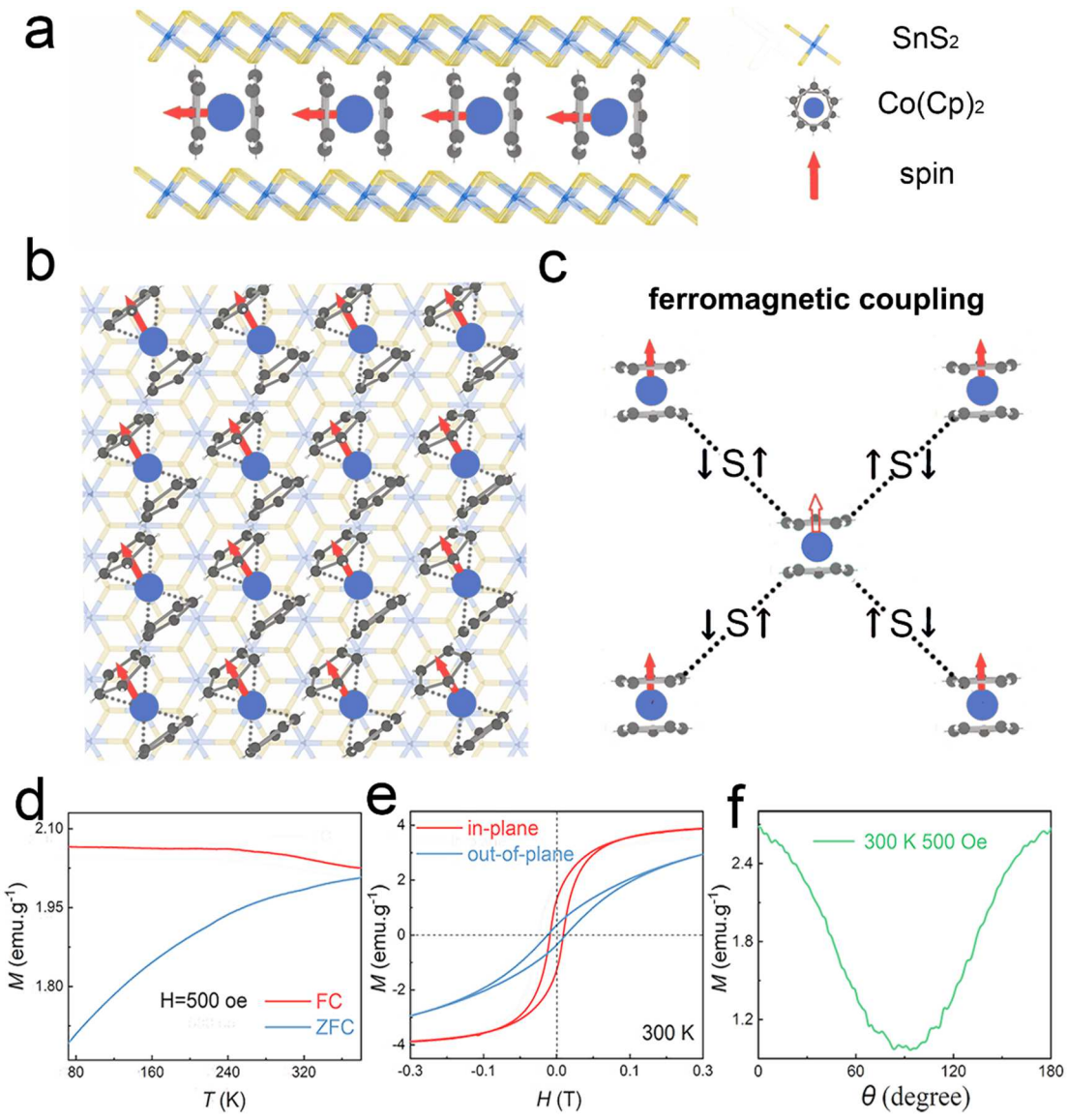

Figure 1: Ferromagnetism of the confined $Co(Cp)_2$ monolayers. a. Scheme for confined $Co(Cp)_2$ between SnS_2 interlayers **b.** Top-view of the $Co(Cp)_2/SnS_2$ structure. **c.** Scheme for the intermolecular vibronic superexchange interaction of adjacent $Co(Cp)_2$ molecules through S atoms. **d.** Magnetization versus temperature under a magnetic field of 500 Oe for ZFC and FC processes. **e.** In-plane and out-of-plane magnetization versus field hysteresis loops at 300 K. **f.** Magnetization versus angle under 500 Oe at 300 K.

Room-temperature ferromagnetic property:

Ferromagnetic molecular monolayers confined in van der Waals (vdW) interlayer space have been synthesized via a solvothermal method. SnS_2 is a typical transition metal dichalcogenide (TMD) possessing a layered structure similar to MoS_2[25]; thus, the 2D interlayers in SnS_2 provide a confined space for limiting the orientation of the structural and spin orders of $Co(Cp)_2$, as shown in the scheme of Fig. 1a. When a heterointerface between organic-2D materials is established, charge transfer plays a role in the formation of organic acceptors on solid surfaces, resulting in strong bonding between the organic molecules and the substrate[26] and leading to anisotropy[27,28]. Thus, a 2D ordered $Co(Cp)_2$ monolayer can be formed in the SnS_2 interlayer space, as shown in Fig. 1b. The dynamic charge transfer from $Co(Cp)_2$ molecules to SnS_2 not only introduces an interaction between adsorbates and the substrate but also

establishes an intermolecular vibronic superexchange effect[29] between two adjacent J-T molecules $Co(Cp)_2$[30,31] through S atoms (Fig. 1c), forming long-range ferromagnetic order.

The room-temperature ferromagnetic signature of $Co(Cp)_2$ layers was affirmed by examining the temperature dependence of magnetization measurements, which were obtained on a vibrating sample magnetometer (VSM). Under a constant magnetic field (H = 500 Oe), field cooling (FC) and zero-field cooling (ZFC) processes were applied to measure the temperature dependence of magnetization (M-T) curves from 70 to 380 K (Fig. 1d). For the FC curve, the magnetization presents a downward trend during the heating process, whereas for the ZFC curve, the magnetization shows an increase with elevating temperature. Note that no intersection exists between the FC and ZFC lines, indicating that the transition temperature of $Co(Cp)_2/SnS_2$ exceeds the range limit of the instrument (380 K). In comparison, the magnetic property measurements of the individual SnS_2 crystal as well as $Co(Cp)_2$ powder show a diamagnetic property and a paramagnetic property, respectively, as displayed in Fig. S1. This result indicates that the ferromagnetic property comes from the combination of $Co(Cp)_2/SnS_2$, namely, confined $Co(Cp)_2$ monolayers. The magnetism of $Co(Cp)_2/SnS_2$ was further studied by taking isothermal magnetization versus field (M-H) curves at 300, 350 and 380 K. The obvious S-shaped curves accompanied by a typical magnetic hysteresis loop (Fig. S2) manifest the room-temperature ferromagnetic property of $Co(Cp)_2$ monolayers.

In addition, the magnetic anisotropy, which is typical characteristics of two-dimensional magnets, can be observed in $Co(Cp)_2/SnS_2$. The in-plane and out-of-plane M-H curves of the sample at 300 K are depicted in Fig. 1e. When the magnetic field is perpendicular to the c-axis of the sample plane, susceptibility saturation can be reached faster than in the vertical case, indicating that the easy magnetization axis (EMA) is along the in-plane direction. To further probe the anisotropy, VSM measurements with a rotator were performed under constant temperature (T = 300 K) and magnetic field (H = 500 Oe). A cosine curve with maxima at $\theta = 0°$ and 180° and a minimum at $\theta = 90°$ is displayed in Fig. 1f, further confirming that the EMA is along the in-plane direction. Based on the above results, we propose a strong ferromagnetic property and magnetic anisotropy in $Co(Cp)_2/SnS_2$ originating from the confined $Co(Cp)_2$ monolayers, implying the successful preparation of a 2D room-temperature ferromagnet.

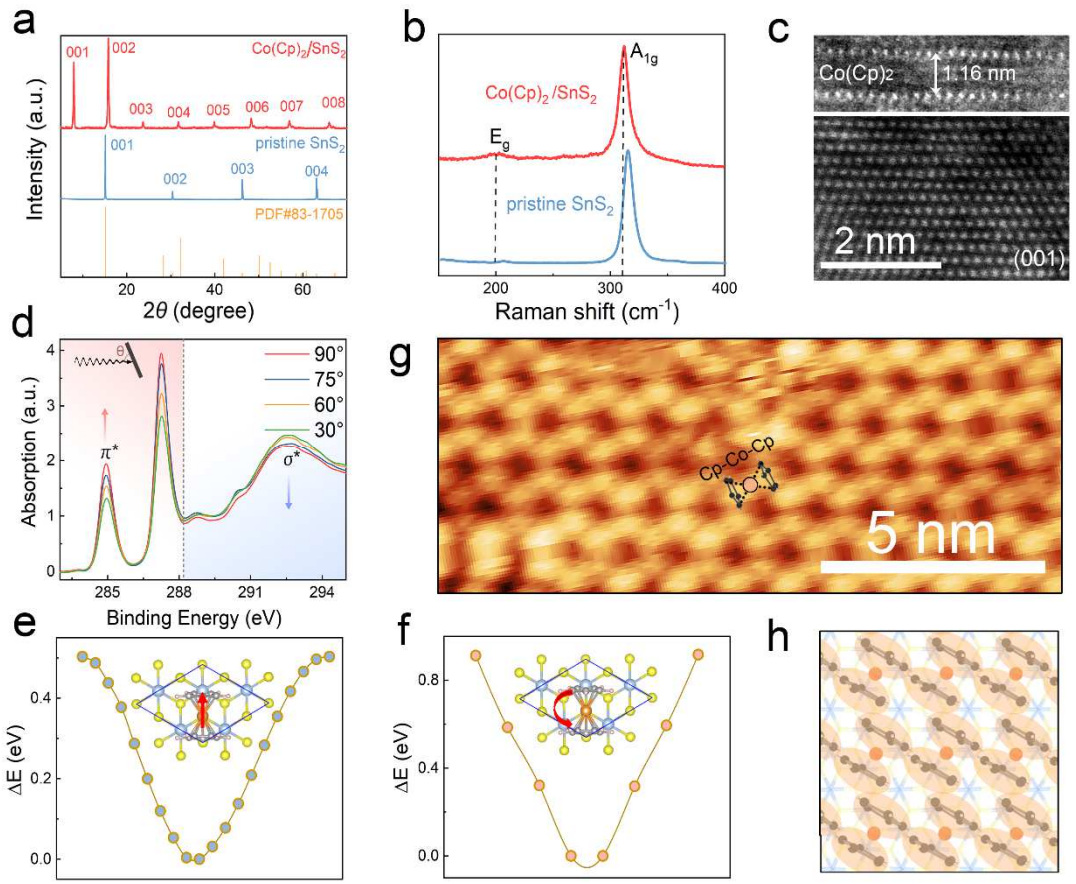

Figure 2: Structure of the confined $Co(Cp)_2$ monolayer. a. XRD patterns of the $Co(Cp)_2/SnS_2$ and pristine SnS_2. **b.** Raman spectrum of a $Co(Cp)_2/SnS_2$ nanoflake and a pristine SnS_2 nanoflake. **c.** HAADF-STEM cross-sectional images of a $Co(Cp)_2/SnS_2$ nanoflake from the side view (top) and top view (bottom). **d.** C K-edge XAS spectra of $Co(Cp)_2/SnS_2$ from 30° to 90°. Potential surface scanning through **e.** translation and **f.** rotation along the high-symmetry direction. **g.** Constant current STM image of a $Co(Cp)_2$ monolayer on a SnS_2 surface. **h.** Scheme of the $Co(Cp)_2$ monolayer on a SnS_2 surface.

Structure of $Co(Cp)_2$ monolayers in SnS_2 interlayers:

The structural of confined molecular was confirmed using a combination of various techniques, as shown in Fig. 2. Owing to the form of $Co(Cp)_2$ layers, the hybrid structure underwent substantial expansion along the [001] zone axis, resulting in a significant increase in the interlayer space, which can be reflected by the powder X-ray diffraction (XRD) pattern in Fig. 2a. After intercalation, the corresponding interlayer distance of $Co(Cp)_2/SnS_2$ increases from 6 Å to 11.6 Å, with an observable peak shift towards lower angles along with a new set of (00l) peaks, showing that the $Co(Cp)_2$ monolayers are in intact SnS_2 interlayers. As shown in Fig. 2b, a slightly redshift is observed in the $Co(Cp)_2/SnS_2$ Raman peaks compared with those of pristine SnS_2. This results from the weakening of the vdW forces induced by the expanded interlayer gap[32], indicating the existence of $Co(Cp)_2$. The interlayer distance of $Co(Cp)_2/SnS_2$ can be specifically measured via high-angle annular dark-field scanning transmission electron microscopy (HAADF-STEM) from the cross section. Using the Z-contrast imaging principle, visually revealing the complete atomic structure in the $Co(Cp)_2/SnS_2$ system, the Sn atoms are found to maintain the same layered parallel arrangement (Fig. 2c). The interlayer distance increases from 5.7 Å to 11.6 Å, which well matches the XRD patterns. In addition, a hexagonal lattice pattern is clearly observed by top-

view HAADF-STEM (Fig. 2c bottom), which well agrees with the SnS_2 template, revealing the retained good crystallinity after the formation of $Co(Cp)_2$ monolayers. The elements, structure and thermal stability of $Co(Cp)_2/SnS_2$ are further shown in Fig. S3-S7. Therefore, through the solvothermal method, $Co(Cp)_2$ monolayers were successfully obtained in the SnS_2 interlayer space.

Due to the aromatic properties of the two characteristic cyclopentadienyl (Cp) rings, the orientation of confined $Co(Cp)_2$ molecules can be revealed using angle-resolved carbon K-edge X-ray absorption near-edge structure (XANES) spectra. The X-ray absorption structure (XAS) spectra for various angles (θ) of the incident light with respect to the $Co(Cp)_2/SnS_2$ plane were collected, as shown in Fig. 2d. The 284.9 and 287.3 eV peaks come from π^* resonances, while the others at 288.7, 290.4 and 292.6 eV originate from σ^* resonances. With increasing θ, the intensity of the π^* resonances shows an uptrend, reaching a maximum at $\theta = 90°$, while the trend of the σ^* resonances is the opposite. The increased intensity of the π^* resonances demonstrates the process in which the incident light and 1s-π^* become parallel, and the decreased intensity of the σ^* resonances reveals a perpendicular tendency, indicating that the Cp axes of $Co(Cp)_2$ molecules are parallel to the SnS_2 plane according to this linear dichroism.

Furthermore, the most stable configuration of confined $Co(Cp)_2$ between SnS_2 interlayers was confirmed with the aid of theoretical studies by scanning the potential energy surface, as shown in Fig. 2e and 2f. To validate the orientation of interlayer $Co(Cp)_2$, we compare the energy of intercalated $Co(Cp)_2$ relative to translational and rotational motions confined in the in-plane direction. By scanning the angular and translational potential energy surface, the initial configuration of interlayer $Co(Cp)_2$ between SnS_2 layers is found to remain the lowest in energy. Moreover, the energy difference between the most stable configuration and the configurations after translational and rotational motions could be as large as 0.50 eV and 0.92 eV, indicating a unified orientation for confined $Co(Cp)_2$ molecules. Based on the above analysis, the orientation of interlayer $Co(Cp)_2$ is confirmed and robust. Thus, ordered 2D arrays can be obtained. A scanning tunnelling microscope (STM) was operated to image the $Co(Cp)_2$ monolayer arrays on SnS_2. As shown in Fig. 2g, all $Co(Cp)_2$ molecules lie flat in a particular direction with the Cp plane erect, which is consistent with the angle-resolved XAS analysis. Particularly, due to the interface rearrangement effect, 2D quasiperiodic arrays of $Co(Cp)_2$ can be observed. The two-lobe symmetrical patterns, representing the double Cp rings, partially overlap, which is consistent with the observed phenomena in previous experiments[33] and reflects the exchange interaction between $Co(Cp)_2$ molecules. The scheme under the STM image shows the arrangement of the confined $Co(Cp)_2$ monolayer more specifically. This molecular order provides favourable conditions for the formation of an intermolecular exchange interaction.

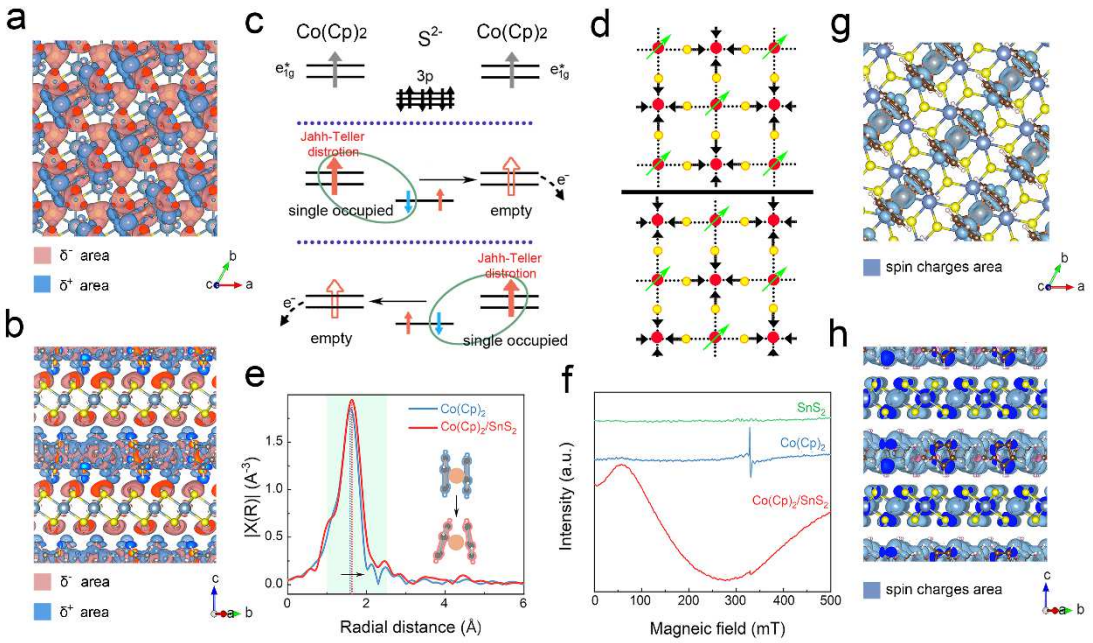

Figure 3：Charge density distribution and ferromagnetic coupling of $Co(Cp)_2$ monolayer. Charge density difference between the SnS_2 substrate and $Co(Cp)_2$ molecules: **a.** top view and **b.** side view. The isosurface values are $4x10^{-3}$ and $1x10^{-3}$ e/bohr^3, respectively. The red area represents the electron-gain (δ^-) area, and the blue indicates the electron-loss (δ^+) area. **c.** Intermolecular vibronic superexchange of $Co(Cp)_2$ via S atoms. **d.** Long-range magnetic ordering in the $Co(Cp)_2$ lattice; the red circle is $Co(Cp)_2$, and the yellow circle is S. **e.** Co FT-EXAFS spectra for isolated $Co(Cp)_2$ (blue) and confined $Co(Cp)_2$ (red). **f.** ESR spectra of pristine SnS_2 (green), $Co(Cp)_2$ (blue) and $Co(Cp)_2$/ $SnSn_2$ (red). Spatial distribution of spin charges for $Co(Cp)_2$/ SnS_2 from the top view **g.** and side view **h**. The isosurface values are $4x10^{-3}$ and $1x10^{-3}$ e/bohr^3, respectively.

Intermolecular vibronic superexchange interaction in the $Co(Cp)_2$ monolayer:

Recently, exchange interactions have been found between two $Ni(Cp)_2$[34,35], which confirms the existence of intermolecular exchange interactions. To better understand the ferromagnetic coupling of confined $Co(Cp)_2$ layer, first-principles calculations were performed to investigate the geometric, electronic and magnetic properties of the intercalated system. As shown in the differential charge density between $Co(Cp)_2$ and the SnS_2 substrate (Fig. 3a, 3b), the electron accumulation and depletion regions are mainly located at the surface S atoms of SnS_2 and the Cp rings, respectively, indicating significant charge transfer between confined $Co(Cp)_2$ and the SnS_2 substrate. Bader charge analysis shows that one Cp molecule could transfer as many as 0.47 e^- electrons to the SnS_2 substrate, and the binding energy of $Co(Cp)_2$ is calculated to be 1.54 eV per $Co(Cp)_2$ molecule, inducing a strong interaction between $Co(Cp)_2$ molecules and the substrate (Table S1 and Fig. S8), thus facilitating unified orientation of confined $Co(Cp)_2$ molecules to form $Co(Cp)_2$ monolayers.

The fact that approximately 0.5 e^- effective average charge transfer, means that half of the $Co(Cp)_2$ will transfer an electron to S at a certain instant (correspondingly become $[Co(Cp)_2]^+$). We proposed that strong ferromagnetic coupling can be achieved in the configuration of $Co(Cp)_2$ -S^{2-}- $[Co(Cp)_2]^+$ in the $Co(Cp)_2$ lattice via intermolecular vibronic superexchange. As the ground state of $Co(Cp)_2$ is $e_{2g}^4\, a_{1g}^2\, e_{1g}^{*1}$ (Fig. S9), with half-filled e_{1g}^* orbital, the J-T effect[36] must be taken into consideration, which leads to structural distortion; while there will be no J-T distortion happened on $[Co(Cp)_2]^+$ with an empty e_{1g}^*

orbital. Owing to the repel and attraction from $Co(Cp)_2$ and $[Co(Cp)_2]^+$, respectively, the middle S^{2-} shift to $[Co(Cp)_2]^+$. Based on the Pauli exclusion principle, exchange coupling can be established between the $Co(Cp)_2$ and $[Co(Cp)_2]^+$ by virtual electron transfer under the framework of superexchange, as shown in Fig. 3c. According to Goodenough–Kanamori rules, there would be ferromagnetic coupling when the virtual electron transfer is from a half-filled to an empty orbital, such as the case of $Co(Cp)_2$ and $[Co(Cp)_2]^+$. Because the J-T distortion is dynamic, the transform between $Co(Cp)_2$ and $[Co(Cp)_2]^+$ is cooperative and in a dynamic equilibrium, which couples the spins of neighboring $Co(Cp)_2$ to form long-range ferromagnetic planes. The mechanism of long-range ferromagnetic order in the $Co(Cp)_2$ monolayer is displayed in Fig. 3d. In addition, the existence of a cooperative dynamic J-T effect in the 2D $Co(Cp)_2$ monolayer generates intrinsic magnetic anisotropy via spin-lattice coupling, achieving 2D ferromagnetism.

To investigate the electronic structure and valence state of confined $Co(Cp)_2$, Co K-edge XANES spectra were obtained. An obvious pre-edge peak at 7730.25 eV can still be observed, suggesting a typical Co-Cp coordination structure, as shown in Fig. S10. The Fourier transform extended X-ray absorption fine structure (FT-EXAFS) spectra reveal a slight increase in the peak position from 1.60 to 1.63 Å, reflecting an increase in the bond length between the central Co atom and the Cp rings, as depicted by the inset in Fig. 3e. Theoretical calculations confirm the twisting of the two Cp rings (Fig. S11), causing the Co-C bond length to be dissimilar and elongate. The breaking of the Cp parallel structure intensifies the anisotropy of $Co(Cp)_2$ and influences the degree of J-T distortion, promoting vibronic superexchange between molecules. Electron spin resonance (ESR) spectra were obtained to detect the magnetic interaction in $Co(Cp)_2$ monolayers. No ESR signal was recorded for the pristine SnS_2 crystal, as shown in Fig. 3f, due to its nonferromagnetic state. The sharp signal at approximately 320 mT in the pure $Co(Cp)_2$ spectrum can be assigned to the signal of Cp rings[37,38]. Of note, this signal is retained in confined $Co(Cp)_2$, reflecting the undestroyed molecular structure for confined $Co(Cp)_2$. However, the signal intensity is greatly reduced compared to pure $Co(Cp)_2$, reflecting the electron transfer from $Co(Cp)_2$ to the SnS_2 layer. In addition, a new broad signal is resolved at approximately 150 mT in the $Co(Cp)_2/SnS_2$ spectrum, which indicates a ferromagnetic interaction in the system, reflecting the ferromagnetism in $Co(Cp)_2$ monolayers.

To provide further insights into the magnetic properties of $Co(Cp)_2$ monolayers, the spatial distribution of spin charges was calculated, as shown in Fig. 3g and 3h. These results show that the spin charge density is mainly contributed by the confined $Co(Cp)_2$ molecule, consistent with the VSM measurement results. The calculated magnetocrystalline anisotropy energy (MAE) for $Co(Cp)_2/SnS_2$, shown in Table S2, indicates that the EMA is parallel to the SnS_2 substrate, along the axial direction of the $Co(Cp)_2$ molecule, and the MAE ranges from 89 to 336 μeV, which stabilizes the long-range magnetic order. To explore the interactions between in-plane molecules, we calculated the orbital-resolved density of states of Cp rings, as shown in Fig. S12. The density of states of the Cp ring is mostly contributed by the in-plane p_x and p_y orbitals, and the spin direction can be inferred to be along the in-plane direction. In addition, the two Cp rings share similar energy levels, reflecting a strong coupling between Cp rings, as shown in Fig. S13. Long-range ferromagnetic ordering in molecular monolayers has been observed in TCNQ arrangements[27]. Thus, a strong intermolecular ferromagnetic interaction between neighbouring $Co(Cp)_2$ molecules, which is responsible for the long-range magnetic order, can be reasonably concluded.

Conclusion

In summary, we have demonstrated a new class of ferromagnetic configurations in confined $Co(Cp)_2$ monolayers that is different from crystalline ferromagnetic systems. Owing to an intermolecular vibronic superexchange interaction, spin order can be realized in $Co(Cp)_2$ monolayers, which is the first room-temperature ferromagnetic molecular monolayer. The vdW interlayer space not only stabilizes molecular monolayers via a confinement effect but also provides interface stress and charge transfer to promote the superexchange interaction between molecules. Our discovery of room-temperature molecular ferromagnetism provides a new way to search for novel ferromagnetic materials and explore exotic properties via intermolecular vibronic superexchange interactions.

Acknowledgement

This work was financially supported by the National Key R&D Program on Nano Science & Technology of the MOST (2017YFA0207301), the National Natural Science Foundation of China (21925110, 21890751, 91745113, 12147105), the National Program for Support of Top-notch Young Professionals, the Fundamental Research Funds for the Central Universities (WK2060190084), the Youth Innovation Promotion Association CAS (2018500), the National Postdoctoral Program for Innovative Talents (BX20190307, BX20190308), the Major Program of Development Foundation of Hefei Centre for Physical Science and Technology (2016FXZY001) and the Users with Excellence Project of Hefei Science Centre CAS (2018HSC-UE002). We appreciate the support from beamline 1W1B of the Beijing Synchrotron Radiation Facility (BSRF, Beijing, China) and beamline BL12B-a of the National Synchrotron Radiation Laboratory (NSRL, Hefei, China). We thank the Cryo-EM Centre at the University of Science and Technology of China for the EM facility support. This work was partially carried out at the USTC Centre for Micro and Nanoscale Research and Fabrication. We gratefully acknowledge the support from the Super Computer Centre of USTCSCC and SCCAS.

Contributions

C.W. conceived the idea, experimentally realized the study, cowrote the paper, supervised the entire project and is responsible for the infrastructure and project direction. Y.G. experimentally realized the study, cowrote the paper and supervised the entire project. Y.L., H.L. and B.Y. contributed equally to this work; they experimentally realized the study, analysed the data and cowrote the paper. These works were assisted by J.P., Y.S., Y.L.Y.Q., and J.Z. HAADF-STEM data collection was performed by Y.L. and X.L. Theoretical calculations were carried out by H.L. and X.W. Y.X. supervised the whole experimental procedure and cowrote the paper. All authors discussed the results and commented on and revised the manuscript.

Competing interests

The authors declare no competing financial interests.

References

1 Gong, C. *et al.* Discovery of intrinsic ferromagnetism in two-dimensional van der Waals crystals. *Nature* **546**, 265-269 (2017).

2 Huang, B. *et al.* Layer-dependent ferromagnetism in a van der Waals crystal down to the monolayer limit. *Nature* **546**, 270-273 (2017).

3 Coomber, A., Beljonne, D., Friend , R. *et al.* Intermolecular interactions in the molecular ferromagnetic $NH_4Ni(mnt)_2 \cdot H_2O$. *Nature* **380,** 144–146 (1996).

4 Goodenough, J. B., Wold, A., Arnott, R. & Menyuk, N. J. P. R. Relationship between crystal symmetry and magnetic properties of ionic compounds containing Mn^{3+}. *Physical Review*, **124(2)**, 373 (1961).

5 Kugel, K. I. & Khomskiĭ, D. J. S. P. U. The Jahn-Teller effect and magnetism: transition metal compounds. *Soviet Physics Uspekhi* **25**, 231 (1982).

6 Englman, R. & Englman, R. The Jahn-Teller effect in molecules and crystals. *John Wiley & Sons* (1972).

7 Aharoni, A. Introduction to the Theory of Ferromagnetism. *Clarendon Press* **109** (2000).

8 Cullity, B. D. & Graham, C. D. Introduction to magnetic materials. *John Wiley & Sons* (2011).

9 Heisenberg, W. Mehrkörperproblem und Resonanz in der Quantenmechanik. *Zeitschrift für Physik* **38**, 411-426 (1926).

10 Dirac, P., On the theory of quantum mechanics. *Proceedings of the Royal Society of London. Series A, Containing Papers of a Mathematical and Physical Character* **112**, 661-677 (1926).

11 Zener, C. Interaction between the d-shells in the transition metals. II. Ferromagnetic compounds of manganese with perovskite structure. *Physical Review* **82**, 403 (1951).

12 Anderson, P. Theory of superexchange interaction. *Physical Review* **79**, 350 (1950).

13 Griffiths, D. J. & Schroeter, D. F. Introduction to quantum mechanics. *Cambridge university press* (2018).

14 Belov, K., *et.al*. Ferromagnetism and antiferromagnetism of rare-earth metals. *Soviet Physics Uspekhi* **7**, 179 (1964).

15 Kasuya, T. A theory of metallic ferro-and antiferromagnetism on Zener's model. *Progress of theoretical physics* **16**, 45-57 (1956).

16 Jonker, G. & Van Santen, J. Ferromagnetic compounds of manganese with perovskite structure. *physica* **16**, 337-349 (1950).

17 Lotgering, F. Ferromagnetism in spinels: CuCr2S4 and CuCr2Se4. *Solid State Communications* **2**, 55-56 (1964).

18 Witte, R. *et al.* High-entropy oxides: An emerging prospect for magnetic rare-earth transition metal perovskites. *Phys. Rev. Mater.* **3**, 034406 (2019).

19 Novoa, J. J., Deumal, M. & Jornet-Somoza, J. Calculation of microscopic exchange interactions and modelling of macroscopic magnetic properties in molecule-based magnets. *Chem. Soc. Rev.* **40**, 3182-3212 (2011).

20 Fukunaga, H. & Miyasaka, H. Magnet design by integration of layer and chain magnetic systems in a pi-stacked pillared layer framework. *ANGEW Chem. Int. Edit* **54**, 569-573 (2015).

21 Ohkoshi, S., *et al.* Magnetic properties of mixed ferro-ferrimagnets composed of Prussian blue analogs. *Phys. Rev. B* **56**, 11642 (1997).

22 Perlepe, P. *et al.* Metal-organic magnets with large coercivity and ordering temperatures up to 242 °C. *Science* **370**, 587-592 (2020).

23 Berezinskii, V. Destruction of long-range order in one-dimensional and two-dimensional systems having a continuous symmetry group I. *Classical systems* **32**, 493-500 (1971).

24 Gibertini, M., *et al*. Magnetic 2D materials and heterostructures. *Nat. Nanotechnol* **14**, 408-419, (2019).

25 Manzeli, S., et al. 2D transition metal dichalcogenides. *Nat. Rev. Mater.* **2**, 33 (2017).

26 Tseng, T. C. *et al.* Charge-transfer-induced structural rearrangements at both sides of organic/metal interfaces. *Nat. Chem.* **2**, 374-379 (2010).

27 Li, Z. *et al.* Confined Synthesis of 2D Nanostructured Materials toward Electrocatalysis. *Adv. Energy Mater.* **10** (2019).

28 Lopez-Cabrelles, J. *et al.* Chemical Design and Magnetic Ordering in Thin Layers of 2D Metal-Organic Frameworks (MOFs). *J Am Chem Soc* **143**, 18502-18510 (2021).

29 Garnica, M. *et al.* Long-range magnetic order in a purely organic 2D layer adsorbed on epitaxial graphene. *Nat. Phys.* **9**, 368-374 (2013).
30 Bersuker, I. B. J. C. r. Modern aspects of the Jahn− Teller effect theory and applications to molecular problems. *Chem. Rev.* **101**, 1067-1114 (2001).
31 Zlatar, M., Schläpfer, C.-W., Penka Fowe, E. & Daul, C. A. Density functional theory study of the Jahn-Teller effect in cobaltocene. *Pure Appl. Chem.* **81**, 1397-1411 (2009).
32 Lee, C. *et al.* Anomalous lattice vibrations of single-and few-layer MoS_2. *ACS. Nano* **4**, 2695-2700 (2010).
33 O'Hare, D. Inorganic and Organometallic Polymers with Special Properties. *Springer, Dordrecht* **191-206** (1992).
34 Czap, G. *et al.* Detection of Spin-Vibration States in Single Magnetic Molecules. *Phys. Rev. Lett.* **123**, 106803 (2019).
35 Czap, G. *et al.* Probing and imaging spin interactions with a magnetic single-molecule sensor. *Science* **364**, 670-673 (2019).
36 Ammeter, J. & Swalen, J. Electronic structure and dynamic Jahn-Teller effect of cobaltocene from EPR and optical studies. *The Journal of Chemical Physics* **57**, 678-698 (1972).
37 Buchalski, P. *et al.* Nickelacyclic-cobaltocene vs. nickelacyclic-nickelocene. Synthesis, X-ray structures, electron transfer activity, EPR spectroscopy, and theoretical calculations. *Inorg. Chem.* **48**, 4934-4941 (2009).
38 Majumdar, M., Saha, S., Dutta, I., Sinha, A. & Bera, J. K. Inter-ligand electronic coupling mediated through a dimetal bridge: dependence on metal ions and ancillary ligands. *Dalton Trans* **46**, 5660-5669 (2017).

Supplementary Files

This is a list of supplementary files associated with this preprint. Click to download.

- SupportinformationRoomTemperatureLongRangeFerromagneticOrderinaConfinedMolecularMonolayer.pdf